J. Synchrotron Rad. (1998). **5**, 562–564

Design of a high-flux and high-resolution VUV bending-magnet beamline

T.-F. Hsieh,* L.-R. Huang, S.-C. Chung, T.-E. Dann, P.-C. Tseng, C. T. Chen and K.-L. Tsang

Synchrotron Radiation Research Center, Hsinchu 300, Taiwan. E-mail: cfs@bl11b.srrc.gov.tw

(*Received 4 August 1997; accepted 11 November 1997*)

A high-flux and high-resolution VUV beamline (4–40 eV) has been designed and is under construction at SRRC. This beamline, which collects 50 mrad of horizontal radiation, uses a 6 m cylindrical-grating monochromator with an incident angle of 70° instead of the conventional normal-incidence-monochromator (NIM) design. Special features, such as movable entrance slit, bendable vertical focusing mirror and movable curved exit slit, are employed to enhance greatly the beamline performance. With both slit openings set at 10 μm, the energy-resolving power can reach as high as 70000. Photon fluxes of 1×10^{13} and 1×10^{10} photons s^{-1} are calculated for energy-resolving powers of 1000 and 40000, respectively. The best image size at the sample position is smaller than 0.45×0.2 mm.

Keywords: beamlines; VUV; high flux; high resolution.

1. Introduction

There is one operational low-energy (6–40 eV) beamline, the 1 m Seya-Namioka monochromator (1 m-SNM), at SRRC (Tseng *et al.*, 1995). However, the total flux of this beamline is less than 1×10^{12} photons s^{-1}, even when both the entrance and exit slits are fully opened. To facilitate experiments of extremely dilute systems or of very low signal-to-noise ratio, it is necessary to construct a high-flux low-energy beamline that can deliver a photon flux greater than 1×10^{13} photons s^{-1}. In addition, a beamline capable of delivering low-energy photons with ultrahigh-energy resolution is also needed for certain types of experiments. In order to meet both requirements, we have decided to construct a high-performance low-energy beamline with the capabilities of providing photons with very high photon flux and ultrahigh-energy resolution. The main design goals of this beamline are (i) it should cover photon energies from 4 to 40 eV, (ii) it should be able to deliver a photon flux greater than 1×10^{13} photons s^{-1} and to provide an ultrahigh-energy resolution capability over the entire energy range, (iii) the image size at the sample position should be less than 0.5×0.5 mm, (iv) adequate floor space should be available for various types of experiment stations, and (v) two separate experiment stations should be operated at the same time to utilize fully the beamtime.

The normal-incidence-monochromator (NIM) design is generally considered for high-flux beamlines in low-energy regions due to its good imaging properties, high-energy resolution and effective rejection of high-order scattered light (Samson, 1967; Wicke *et al.*, 1983; Eyers *et al.*, 1983; Lama *et al.*, 1994; Suits *et al.*, 1995; Heimann *et al.*, 1997). However, at normal incidence the reflectivity of all materials is extremely low at photon energies above ~25 eV (Windt *et al.*, 1988). Besides, it is very difficult for an NIM to provide sufficient floor space for various types of experimental stations due to its awkward geometric arrangement. On the other hand, the Dragon-type SGM beamline (Chen, 1987) equipped with a proper gas cell system can meet all our expectations. Therefore, we have chosen the 6 m cylindrical-grating monochromator (6 m-CGM) design with an incident angle of 70° instead of the conventional NIM design. A gas cell with a special differential pumping system will be used to reject the high-order scattered light. A detailed description of the differential pumping system will be presented elsewhere (Chen *et al.*, 1998).

2. Optical system

The optical layout of the 6 m-CGM high-flux beamline is shown in Fig. 1 and the parameters of the optical components are listed in Table 1. Similar to the Dragon-type beamlines, a 6 m-CGM is arranged between pre-focusing and post-focusing mirrors. In order to maximize the beamline performance, we have adopted several special features including a modified plane-elliptical horizontal pre-focusing mirror (HFM), a bendable vertical pre-focusing mirror (VFM), two movable slits, and a curved exit slit. The beamline components and the special features are described in the following.

The HFM, which is located at 3.2 m from the source, collects 50 mrad of the horizontal radiation fan. Since a thermal loading of 200 W will be deposited on this mirror, the HFM is internally water-cooled. The photon beam is horizontally focused onto a location between the entrance slit (S_1) and the exit slit (S_2) in order to keep the image size at either slit less than 7 cm. The HFM is a specially designed plane-ellipse. The shape of the ellipse is calculated directly from the geometry of the optical arrangement and the actual shape of the radiation source (Chen *et al.*, 1998). The radiation source is a 20 cm-long arc strip which is a section of the electron orbit in the bending magnet. Unlike the normal plane-elliptical surface which focuses a point source into a line, the modified plane-elliptical surface can focus an arc-strip source into a line perpendicular to the plane of the arc. This modified plane-elliptical surface can thus eliminate the large aberration effect caused by the large horizontal source size when using a normal plane-elliptical surface and hence provide perfect focusing in the horizontal plane. The surface figure of the modified plane-ellipse is defined by an eighth-degree polynomial surface height function, $y = \sum_{n=2}^{8} c_n x^n$. Thanks to recent advances in beamline optical

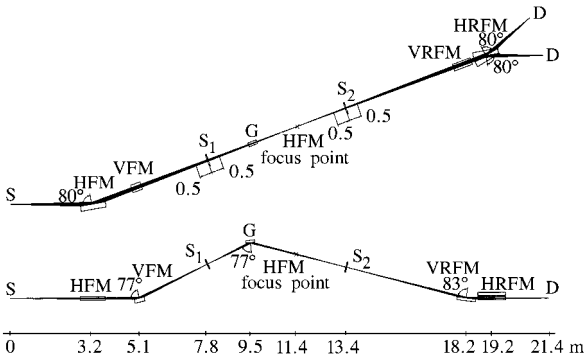

Figure 1
Optical layout of the 6 m-CGM high-flux beamline. S, radiation source; HFM, horizontal pre-focusing mirror; VFM, vertical pre-focusing mirror; S_1, entrance slit; G, gratings; S_2, exit slit; VRFM, vertical refocusing mirror; HRFM, horizontal refocusing mirror; D, sample position.

Table 1
Optical parameters of the 6 cm-CGM high-flux beamline.

	Horizontal pre-focusing mirror HFM	Vertical pre-focusing mirror VFM	Entrance slit S_1 Entrance slit S_2	Grating G	Vertical refocusing mirror VRFM	Horizontal refocusing mirror HRFM1/2
r_1 (mm)	3200	5100		1929	5006	8397
r_2 (mm)	8729	3000 ± 500		4071	3250	2250
Deviation angle (°)	160	154		140	166	160
Type	Plane ellipse (modified) (water-cooled)	Cylinder (bendable)	Bilaterally adjustable Circularly curved S_2	Cylinder	Sphere	Plane ellipse
Size (mm)	100 × 75 × 100	200 × 150 × 50	H: 5–70, V: 0–3	120 × 50 × 30	550 × 180 × 70	1000 × 60 × 100
Coating	Al + MgF_2	Al + MgF_2		Al + MgF_2	Al + MgF_2	Al + MgF_2
Substrate	Glidcop	ULE		ULE	ULE	ULE
Curvature (mm)	Polynomials $a + a'$, $b + b'$	16793.8 (14900–18500)	5200 (S_2)	8510	32340	a = 5323.3, b = 754.8
Ruling profit				Laminar mask 1:1		
Ruling density (mm^{-1})				450 800 1600		
Ruling depth (Å)				800 450 250		

technology, the modified plane-ellipse is now commercially available.

The VFM is a bendable cylindrical mirror, whose radius can be continuously changed so that the photon beams can always be focused vertically onto the movable entrance slit. The entrance slit is made movable to enhance greatly the energy resolution. Three cylindrical gratings, 450, 800 and 1600 lines mm^{-1}, are used to cover photon energies from 4 to 40 eV. Gratings with a cylindrical reflection surface are chosen to reduce the aberration caused by the large horizontal angular acceptance (50 mrad). A laminar ruling profile is used for each grating to reduce the efficiency of high-order scattered light. Due to the large horizontal angular acceptance, the focused image is curved for the entire energy range, but can be represented by a simple circular arc with a radius of 5.2 m. Therefore, a curved slit jaw is used to improve further the flux and the resolution. One spherical refocusing mirror, VRFM, is used to focus the beams vertically onto the sample. A regular plane-elliptical mirror, HRFM, located after the VRFM is employed to focus from the HFM focal point onto the sample. The best focused spot at the sample position is smaller than 0.45 × 0.2 mm. The vertical spot size at the sample position changes from 0.2 mm to 0.6 mm with different exit-slit positions. Two HRFMs are used for delivering the photon beam to two separate experimental stations.

3. Estimated performance

Following the Dragon beamline design criteria (Chen, 1987), the performance of the 6 m-CGM is optimized. An incident angle of 70° is chosen and the sum of the entrance arm and exit arm is set at roughly 6 m for the monochromator to maximize the energy resolution and photon throughput. In order to reduce the resolution limits, cylindrical gratings are used to minimize the astigmatic coma term (C_{12}) and astigmatic term (C_{02}), and a movable exit slit is used to eliminate the defocus term (C_{20}). A radius of 8.51 m is chosen for the grating to match the monochromator parameters and optimize the resolution. If the entrance slit is kept fixed, the resolution may be limited by the coma term (C_{30}) in some energy range. The resolving power of the fixed-entrance-slit 6 m-CGM calculated using the *SHADOW* ray-tracing programs (Lai & Cerrina, 1986) is shown in Fig. 2(*a*). In this calculation, the opening of both slits is 10 μm and the slope error of the grating surface is ±0.1 arcsec. The resolving power of each grating has a maximum in the middle and falls off on both sides. The resolving power can be further improved by eliminating the C_{30} term. By moving both the entrance and exit slit to satisfy the Rowland-circle focusing conditions (Samson, 1967; Hogrefe *et al.*, 1986), *i.e.* $r_1 = R\cos\alpha$ and $r_2 = R\cos\beta$, both the C_{20} and C_{30} terms can be eliminated simultaneously. Fig. 2(*b*) displays the resolving powers under this condition, showing a maximum value of 70000.

The photons from the bending-magnet radiation source are composed of *p*-polarization and *s*-polarization components. The reflectance of each polarization component is different, and thus it should be considered separately. For example, the reflectivity of the *p*-polarization component at photon energy 10 eV is about 20% lower than that of the *s*-polarization component, if an aluminium-coated mirror faces horizontally, such as the HFM, and the incident angle of the photon beam is 80°. The polarization-

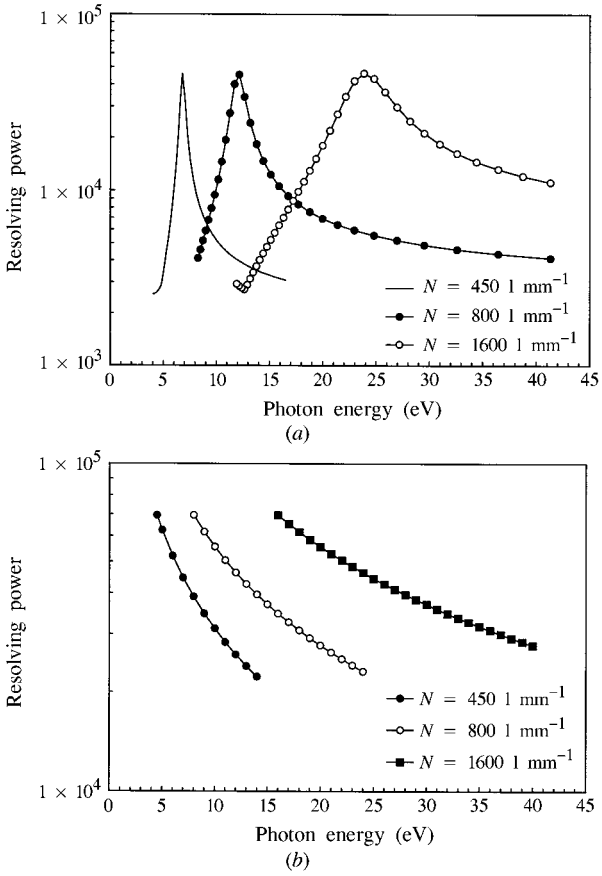

Figure 2
Calculated resolving power of each grating, (*a*) with a fixed entrance slit and a movable exit slit, and (*b*) with both slits movable to meet the Rowland-circle conditions. In these calculations, both slits are set at 10 μm.

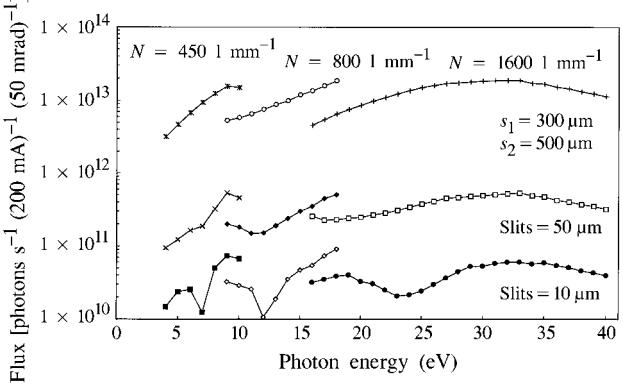

Figure 3
Calculated photon flux for each grating and various slit openings.

dependent reflectance of all the optical surfaces, mirrors and gratings can be calculated using the Fresnel equations and the tabulated refraction coefficients, n and k (Marr, 1987; Windt *et al.*, 1988). The calculated photon fluxes for different gratings and slit openings are shown in Fig. 3. With a storage-ring current of 200 mA, photon fluxes of 1×10^{13} and 1×10^{10} photons s^{-1} are expected for energy-resolving powers of 1000 and 40000, respectively.

4. Summary

A very high photon flux and ultrahigh-resolution low-energy beamline, covering photon energies from 4 to 40 eV, has been designed. In addition to the conventional 6 m-CGM design, several special features, such as the specially designed plane-ellipse mirror, the bendable vertical focusing mirror, the movable entrance slit and exit slit, and the curved exit slit jaw, are utilized to enhance greatly the beamline performance. The expected photon fluxes are greater than 1×10^{13} and 1×10^{10} photons s^{-1} for energy-resolving powers of 1000 and 40000, respectively, even after taking into account the polarization effect on reflectance. The best focused spot at the sample location is less than 0.45 × 0.2 mm. This beamline is currently under construction at SRRC and will be ready for commissioning in the spring of 1998.

We would to thank Dr Li-Jin Lu at HESYRL for useful discussions on the polarization effect.

References

Chen, C. T. (1987). *Nucl. Instrum. Methods*, A**256**, 595–604.
Chen, C. T. *et al.* (1998). In preparation.
Eyers, A., Heckenkamp, Ch., Schafers, F., Schonhense, G. & Heinzmann, U. (1983). *Nucl. Instrum. Methods*, **208**, 303–305.
Heimann, P. A., Koike, M., Hsu, C. W., Blank, D., Yang, X. M., Suits, A. G., Lee, Y. T., Evans, M., Ng, C. Y., Flaim, C. & Padmore, H. A. (1997). *Rev. Sci. Instrum.* **68**, 1945–1951.
Hogrefe, H., Howells, M. R. & Hoyer, E. (1986). *Proc. SPIE*, **733**, 274–285.
Lai, B. & Cerrina, F. (1986). *Nucl. Instrum. Methods A*, **246**, 337–341.
Lama, F., Derossi, A., Piacentini, M. & Zema, N. (1994). *Nucl. Instrum. Methods Phys. Res. A*, **339**, 610–616.
Marr, G. V. (1987). *Handbook on Synchrotron Radiation*, Vol. 2, pp. 41–52. Amsterdam: North-Holland.
Samson, J. A. (1967). *Techniques of VUV Spectroscopy*, pp. 43–84. Lincoln, Nebraska: Pied.
Suits, A. G., Heimann, P., Yang, X., Evans, M., Hsu, C.-W., Lu, K. & Lee, Y. T. (1995). *Rev. Sci. Instrum.* **66**(10), 4841–4844.
Tseng, P.-C., Hsieh, T.-F., Song, Y.-F., Lee, K.-D., Chung, S.-C., Chen, C.-I., Lin, H.-F., Dann, T.-E., Huang, L.-R., Chen, C.-C., Chung, J.-M., Tsang, K.-L. & Chang, C.-N. (1995). *Rev. Sci. Instrum.* **66**(2), 1815–1817.
Wicke, H., Bohmer, W. & Schwentner, N. (1983). *Nucl. Instrum. Methods*, **204**, 533–542.
Windt, D. L., Csah, W. C., Scoot, M., Arendt, P., Newnam, B., Fisfer, R. F., Swartzlander, Takacs, P. Z. & Pinneo, J. M. (1988). *Appl. Opt.* **27**(2), 279–295.